Extended Data Figures

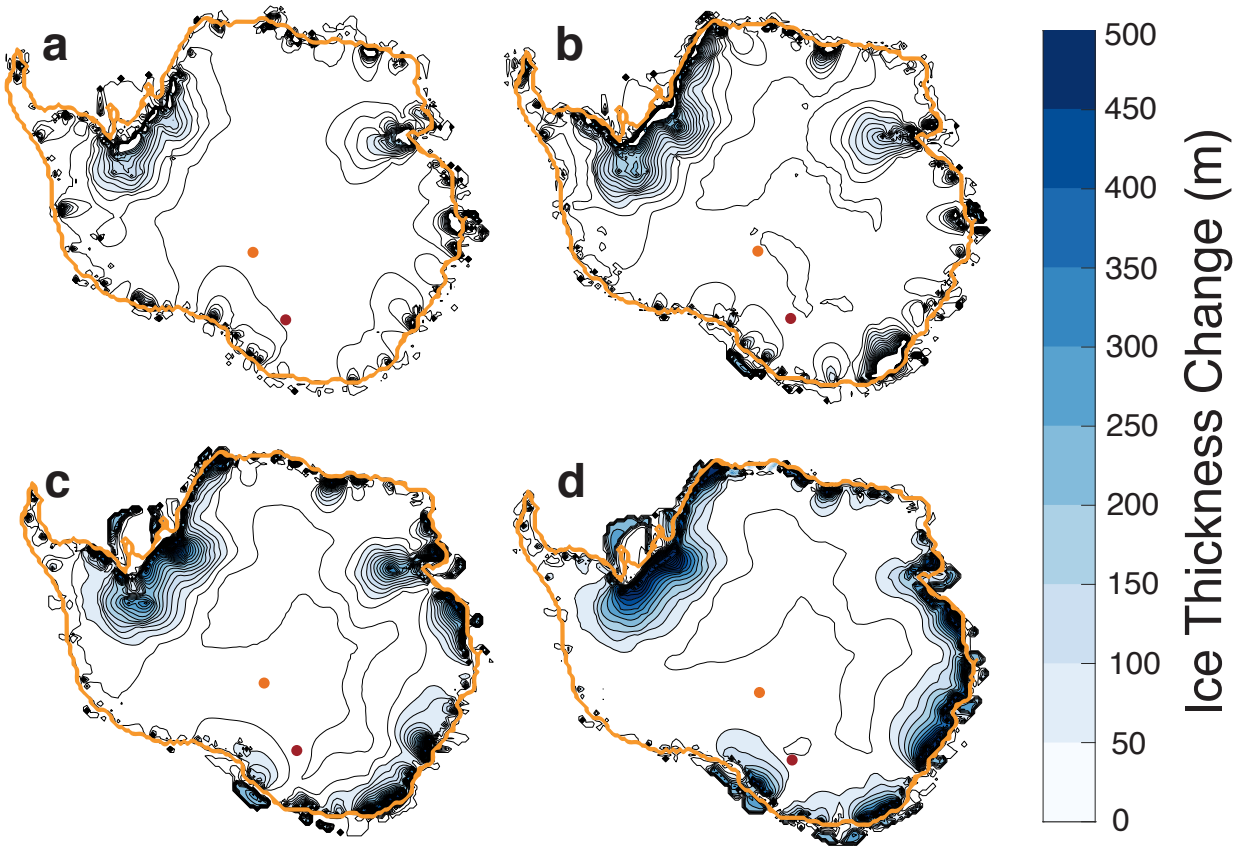

Extended Data Fig. 1 | Modeled Antarctic Ice Sheet Thickness Change between Cold and Warm Climate Phases Using Different Ocean–Ice Heat Flux Values. a. Contour plot of AIS thickness change from ocean forcing with an ocean–ice heat flux value of 1 m a^{-1} K^{1}. Contour interval is 15 m. Under these conditions, Antarctica would contribute <1 m sea level equivalent during millennial climate cycles **b.** As is **a.** with an ocean–ice heat flux value of 3 m a^{-1} K^{1}. Under these conditions, Antarctica would contribute between <1 m and 2.5 m sea level equivalent during millennial climate cycles **c.** As is **a.** with an ocean–ice heat flux value of 5 m a^{-1} K^{1} and contour interval of 25 m. Under these conditions, Antarctica would contribute between 1.5 m and 3 m sea level equivalent during millennial climate cycles **d.** As is **a.** with an ocean–ice heat flux value of 7 m a^{-1} K^{1} and contour interval of 50 m. Under these conditions, Antarctica would contribute between 2.5 m and 5 m sea level equivalent during millennial climate cycles. Markers show collection locations of samples MA113 (orange) and PRR50489 (red). Yellow line delineates the grounding line during millennial cold period.

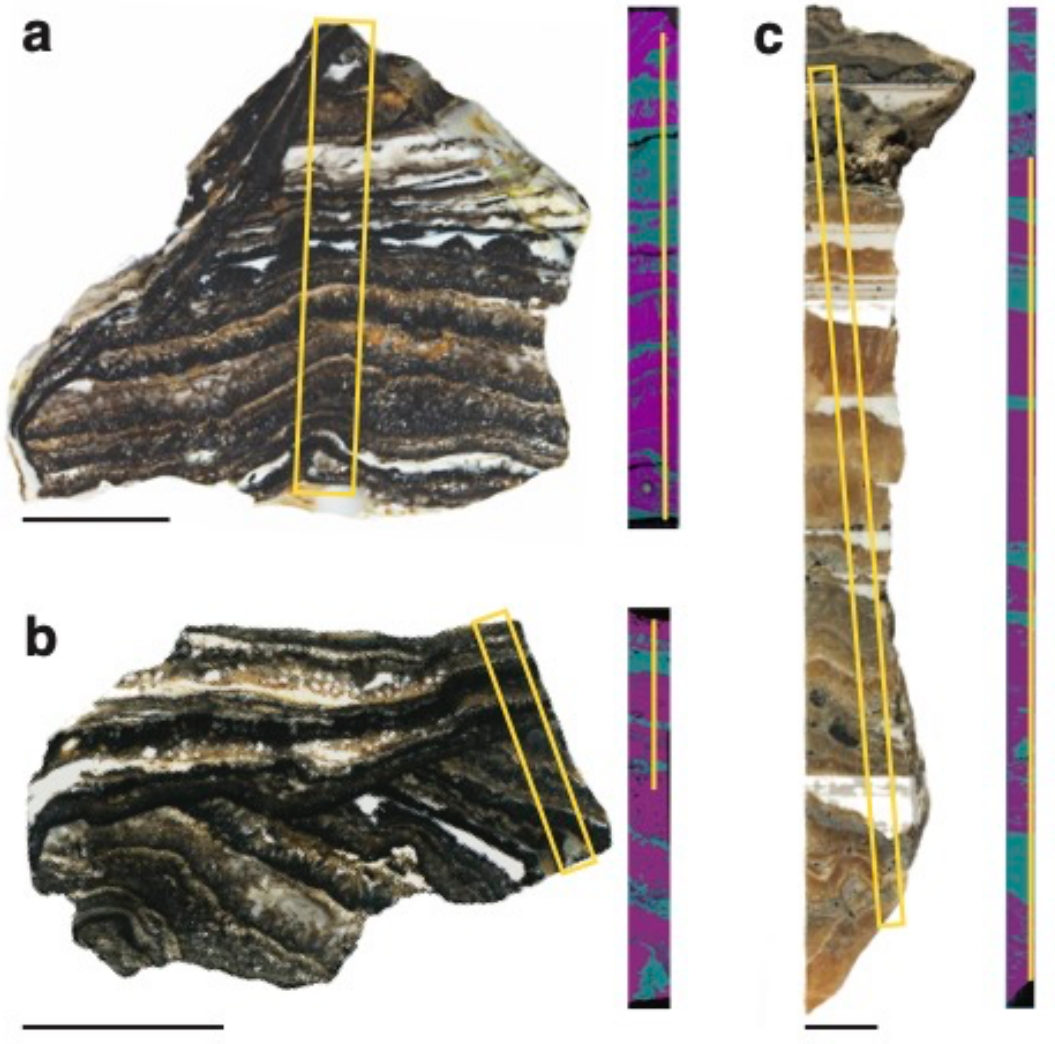

Extended Data Fig. 2 | Slab and SEM-EDS images of precipitates PRR50489 and MA113. a. Slab and SEM-EDS image of sample PRR50489. **b.** Slab and SEM-EDS image of second piece of sample PRR50489. This piece of sample includes material above angular unconformity. **c.** slab and SEM-EDS image of sample MA113. Yellow boxes on slab images outline areas where SEM images were taken. Yellow lines on SEM images indicate position of line scan for spectral outputs in figure 2. SEM-EDS images show Ca concentration (i.e., calcite) in pink and Si concentration (i.e., opal) in teal.

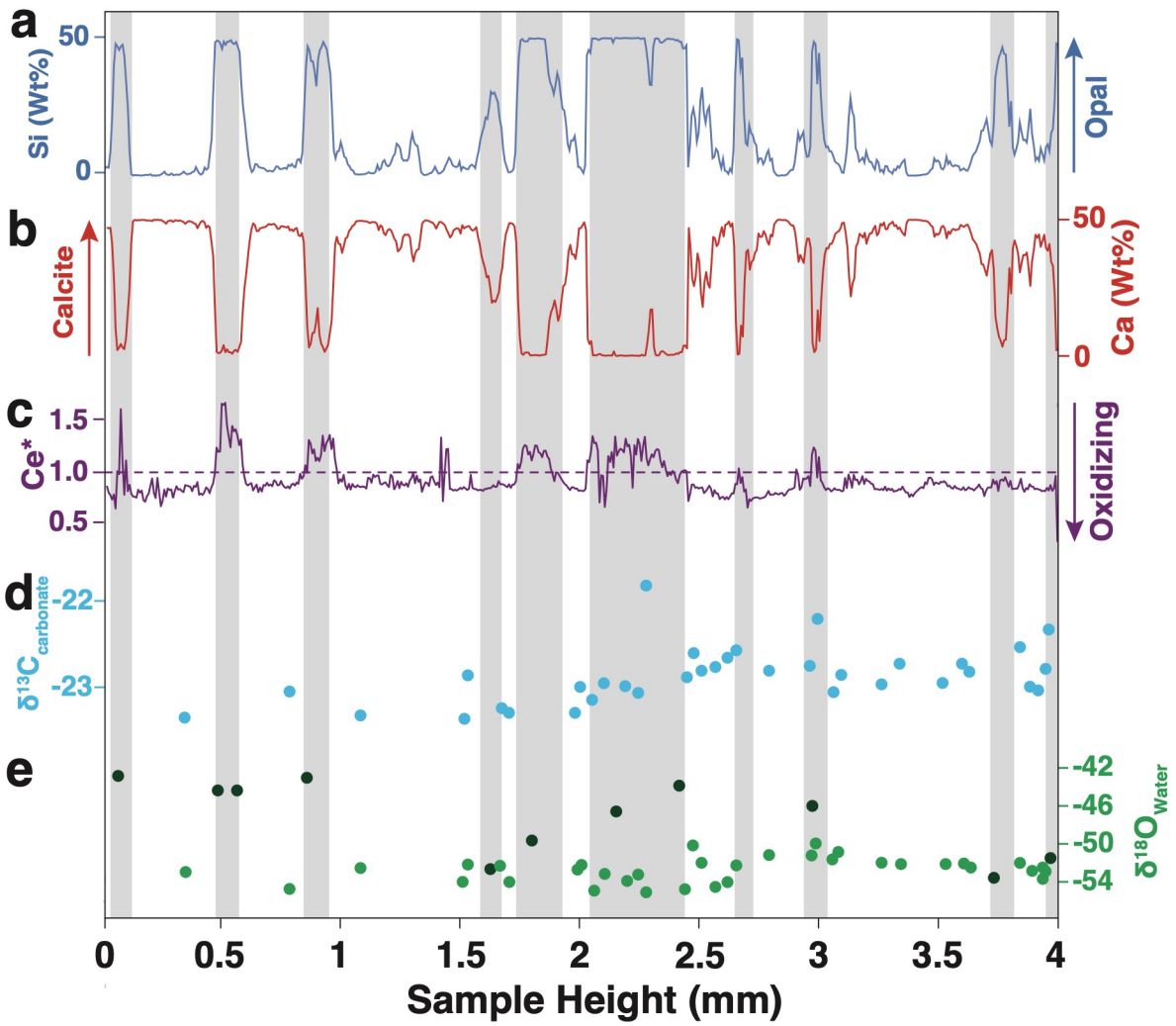

Extended Data Fig. 3 | Geochemical Data from PRR50489. a. LA ICP-MS Si concentration curve **b.** LA ICP-MS Ca concentration curve **c**. LA ICP-MS Ce* curve **d**. $\delta^{13}C$ data from calcite layers **e**. $\delta^{18}O$ data from calcite (light green) and opal (dark green) layers. Opal layers are represented by areas with high Si and low Ca concentrations and grey bars; calcite layers have high Ca concentration and low Si concentration and are represented by white bars.

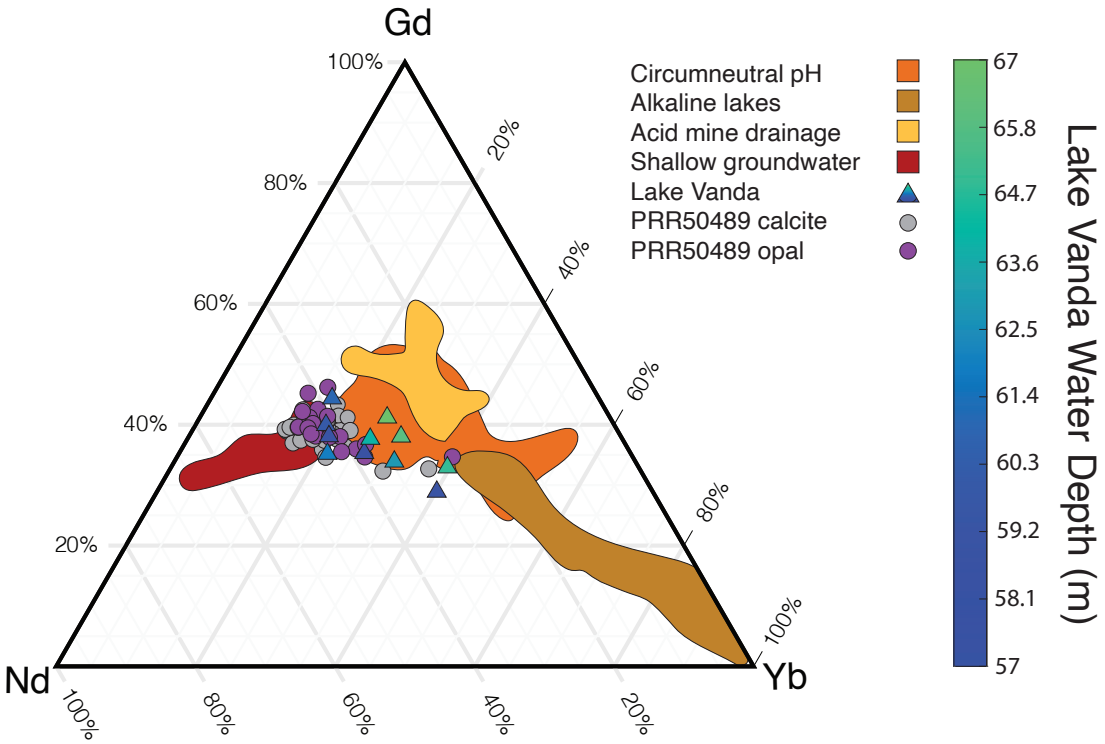

Extended Data Fig. 4 | Rare Earth Element Ternary Plot. Ternary plot with Rare Earth Elements gadolinium, neodymium, and ytterbium. Filled areas plot compositional range for different surface and groundwaters after ref.[1]. Triangles represent Lake Vanda water compositions colored based on depth from 57m to 67m depth[2]. PRR50489 calcite and opal compositions are plotted as black and blue spheres respectively. PRR50489 data were collected using LA ICP-MS.

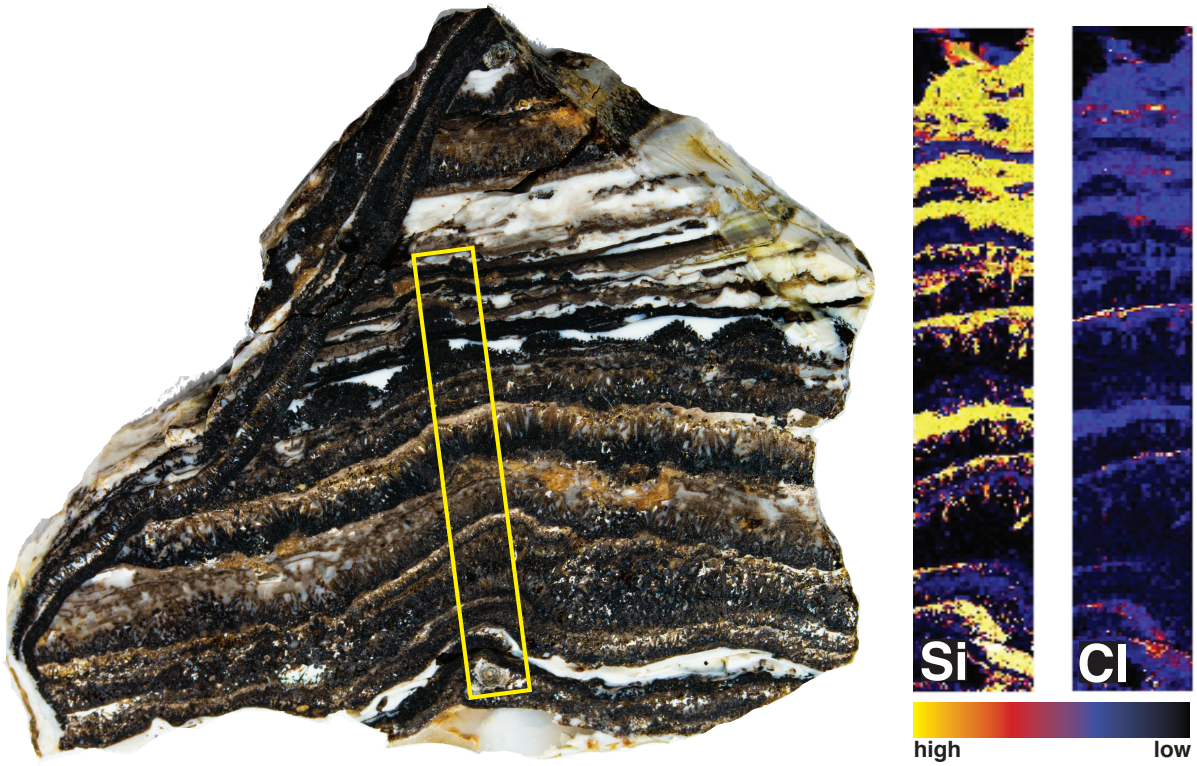

Extended Data Fig. 5 | Synchrotron X-Ray fluorescence maps from sample PRR50489. a. Slab image of sample PRR50489. Yellow box outline area of X-Ray florescence measurements in **b. b.** X-Ray florescence maps of Si and Cl from the Tender Energy Spectroscopy (TES) beamline at the National Synchrotron Light Source II (NSLS II).

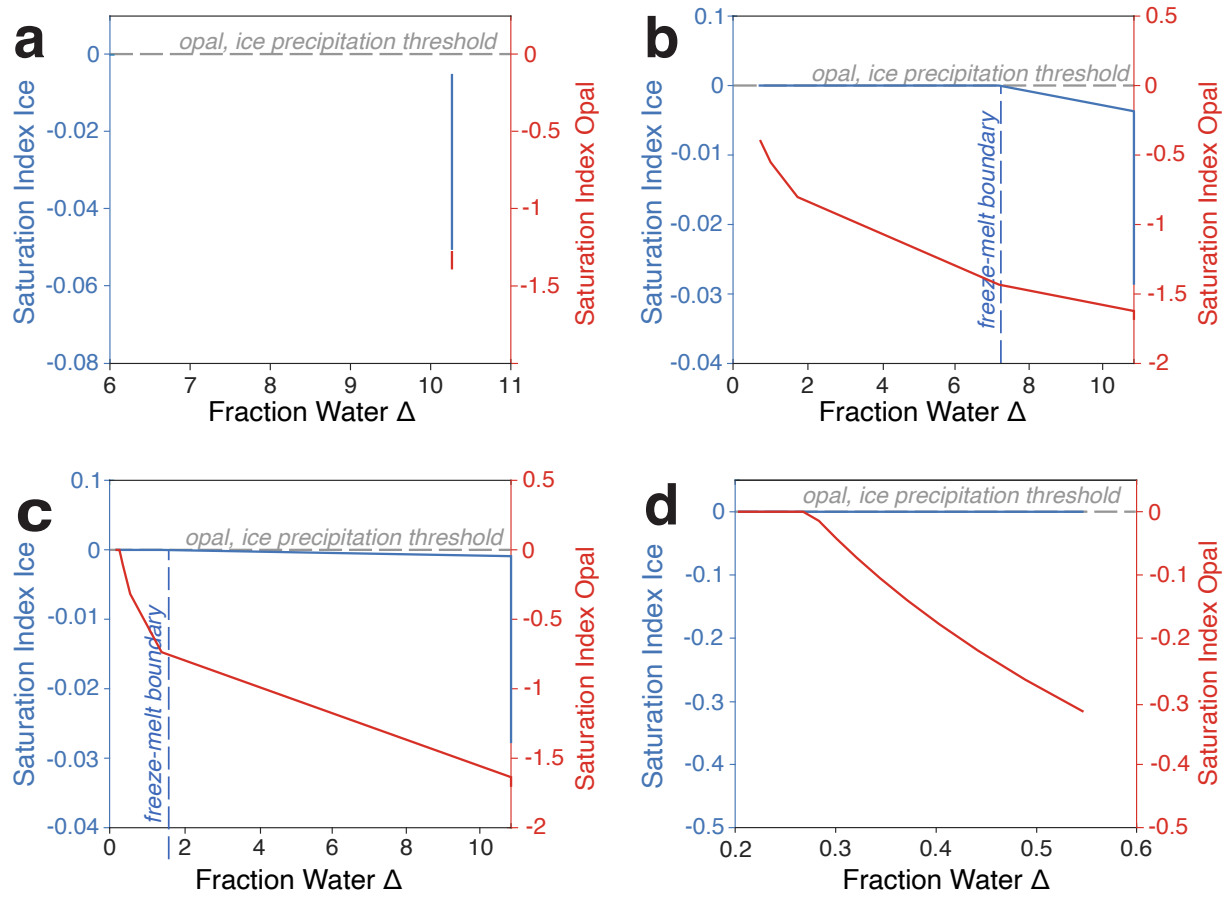

Extended Data Fig. 6 | Model simulations predicting opal formation from $CaCl_2$ brine. PHREEQC simulations of cryoconcentration of Don Juan Pond (DJP) $CaCl_2$ brine[3,4] over a range of temperatures and relative concentrations. X-axes show the relative fraction of water that enters the system (as meltwater) or leaves the system (as ice) upon equilibration of the brine with the overlying ice. Fraction water Δ values above 1 indicate meltwater addition; fraction water Δ values below indicate water loss via freezing. Si concentration of brine is assumed to match that of average global surface waters at 14ppm[5]. Plots show saturation indices (SI) — the log ratio of the ion activity product and equilibrium constant — of ice (blue) and opal (red). SI values greater than 0 are supersaturated with respect to that phase; values less than 0 are undersaturated. The grey, dashed lines delineate SI precipitation threshold for opal and ice. Saturation indices of calcite are not shown because the lack of carbon in DJP brine makes the solution unsaturated with respect to calcite **a.** Equilibration of concentrated DJP brine with ice and opal over a range of temperatures between -5 and 5˚C. High ionic strengths in the concentrated brine causes significant melting of overlying ice, diluting the solution with respect to opal, and inhibiting opal precipitation. **b.** Equilibration of 10x diluted DJP brine with ice and opal over a range of temperatures between -5 and 5˚C. In this case the brine starts to freeze at -2˚C, but the solution does not reach opal precipitation because the degree of freezing (i.e., cryoconcentration) of Si is suppressed by the high ionic strength of the brine. **c.** Equilibration of 50x diluted DJP brine with ice and opal over a range of temperatures between -5 and 5˚C. This solution also reaches freezing at -2˚C, but the relatively lower ionic strength allows more significant portions of cryoconcentration of Si, causing

opal to precipitate near -3.5˚C **d.** Equilibration of 50x diluted DJP brine with ice and opal over a smaller range of temperatures, between -4 and -3˚C. This plot shows that opal precipitation occurs when ~75% of the water is lost via freezing, which occurs at ~ -3.5˚C.

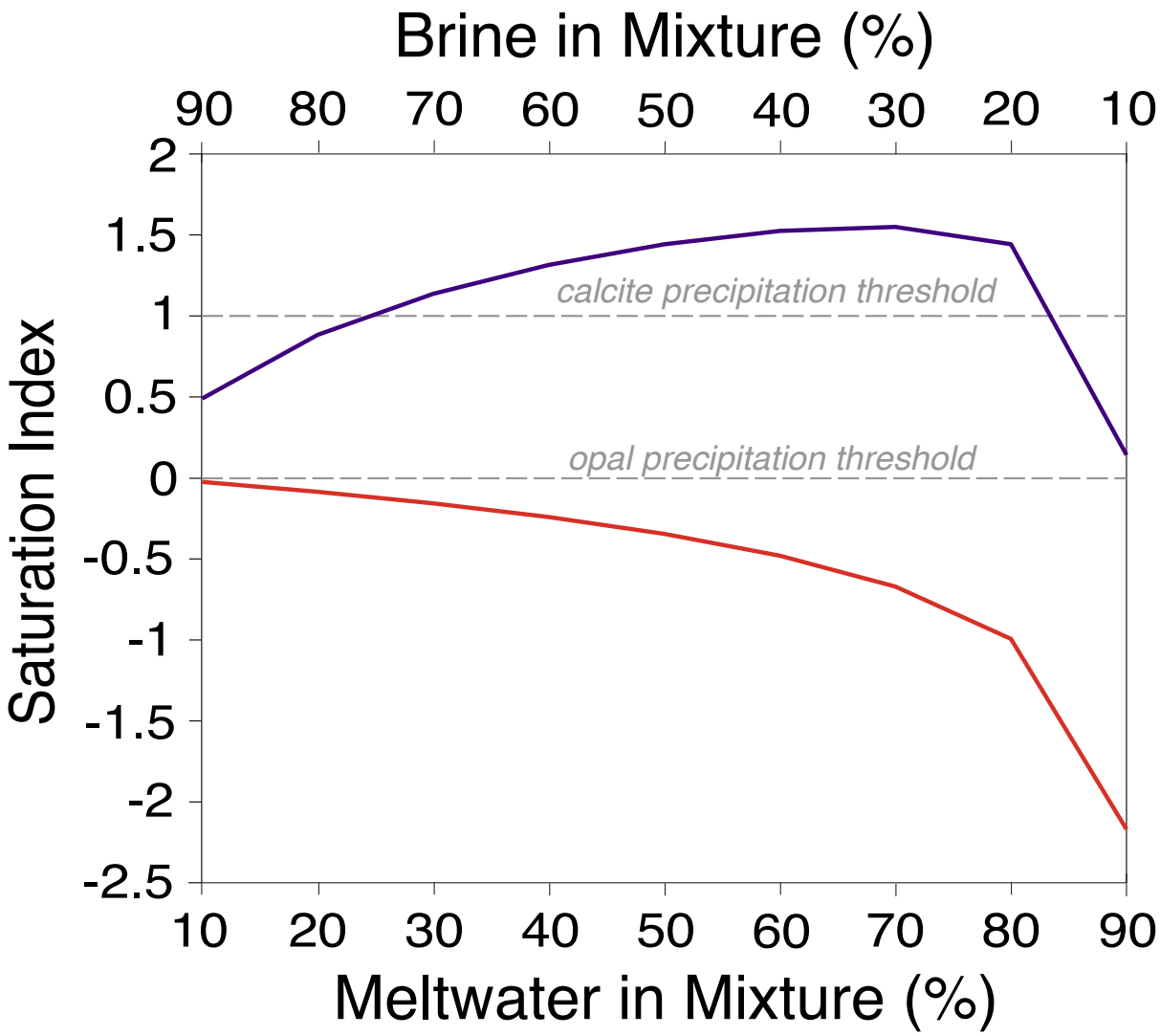

Extended Data Fig. 7 | Model simulations predicting calcite formation via mixing of meltwater and $CaCl_2$ brine. PHREEQC simulations of a range of mixing ratios between $CaCl_2$ brine and Casey Station jökulhlaup water. Brine starting temperature is set at -3.5˚C matching ideal conditions for opal precipitation shown in Extended Data figure 5; meltwater starting temperature is at -1.5˚C based on the amount of heat added to the system by shear heating in our reduced complexity ice sheet model. Calcite precipitation threshold is defined by the observation that calcite precipitation can be inhibited until strong supersaturation[6,7]. Plot shows that meltwater addition halts opal precipitation (red curve), while generating calcite precipitation (purple curve) in a mixing ratio between 30:70 and 80:20 meltwater to brine.

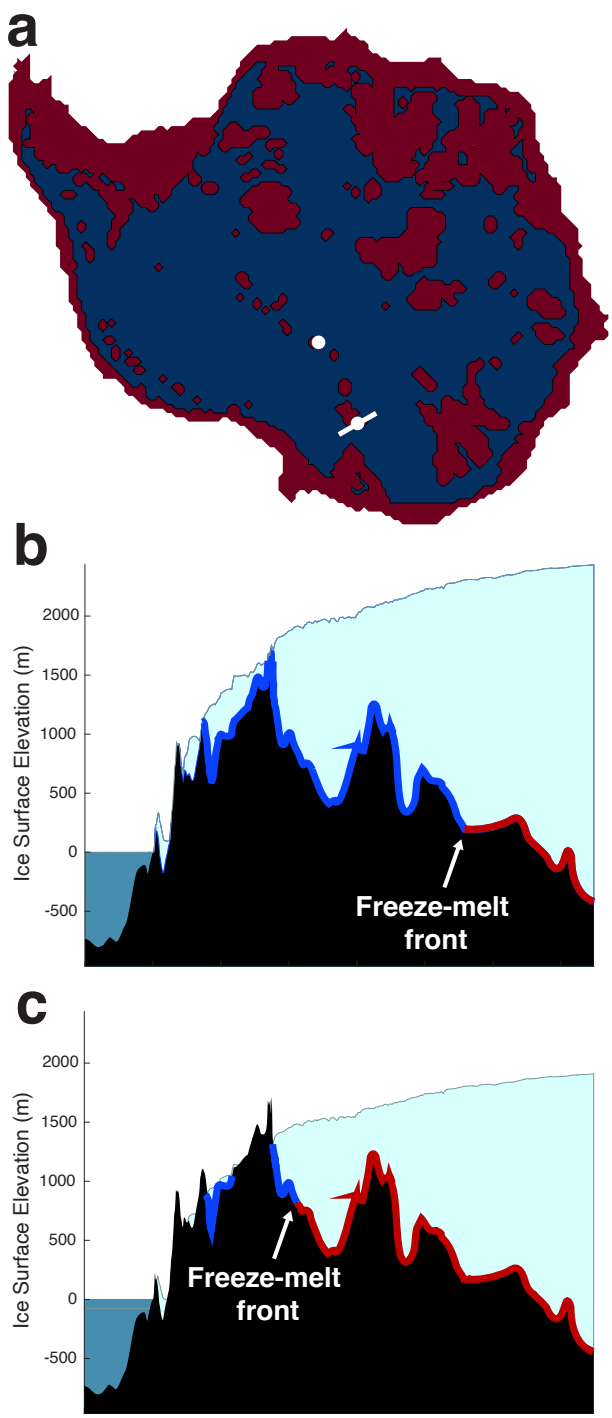

Extended Data Fig. 8 | Schematic of subglacial hydrologic change during millennial climate cycles. a. Modeled basal melting conditions during the Late Pleistocene[8]. Red areas indicate basal freezing; blue areas indicate basal melting. White marker indicates sample collection locations; line delineates transect of bedrock topography shown in **b**. and **c. S**ample locations along Transantarctic Mountains are close to the transition between basal freezing and melting. **b.** Bedrock topographic transect[9] (black) between the Ross Sea (teal) and the Wilkes basin, with ice sheet thickness representative of conditions during Antarctic cold periods. **c.** Bedrock topographic transect[9] (black) between the Ross Sea (teal) and the Wilkes basin, with thinner ice sheet representative of conditions during Antarctic warm periods. Dark blue areas along bedrock-ice sheet interface represents areas of subglacial freezing, red areas represent subglacial melting. We hypothesize that freeze-melt front migrates further inland during periods of cold Antarctic climate (as in **a**) and towards the Ross Sea during periods warm Antarctic climate (as in **b**). Ice sheet thickness changes, shown on y-axis are estimated based on model outputs shown in figure 2.

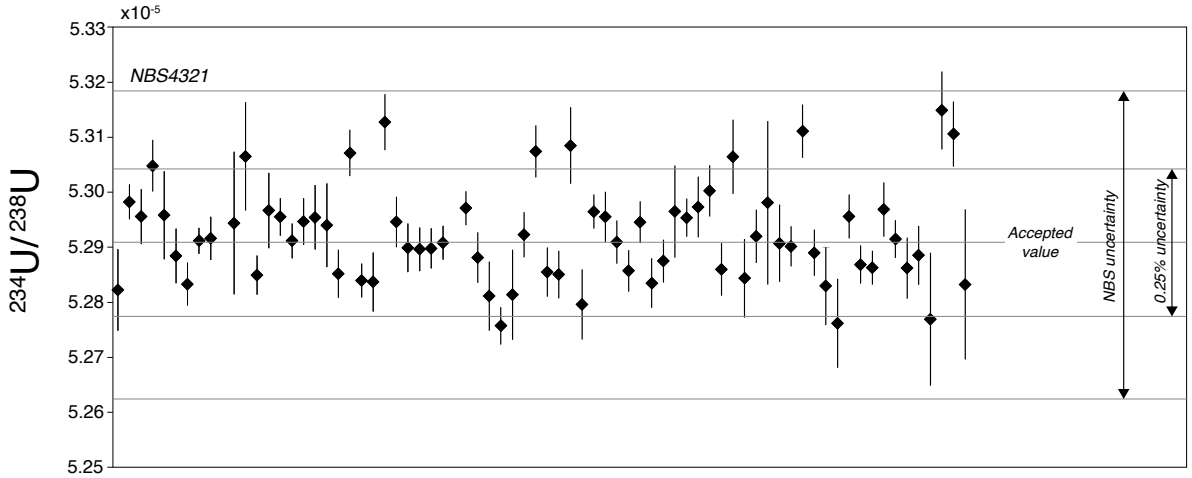

Extended Data Fig. 9 | Long-term results of measurements of NBS 4321 ($5.2919 \times 10^{-5} \pm 0.013 \times 10^{-5}$ (0.25%)) at UCSC using an IsotopX X62, TIMS. All uncertainties are absolute 2σ.

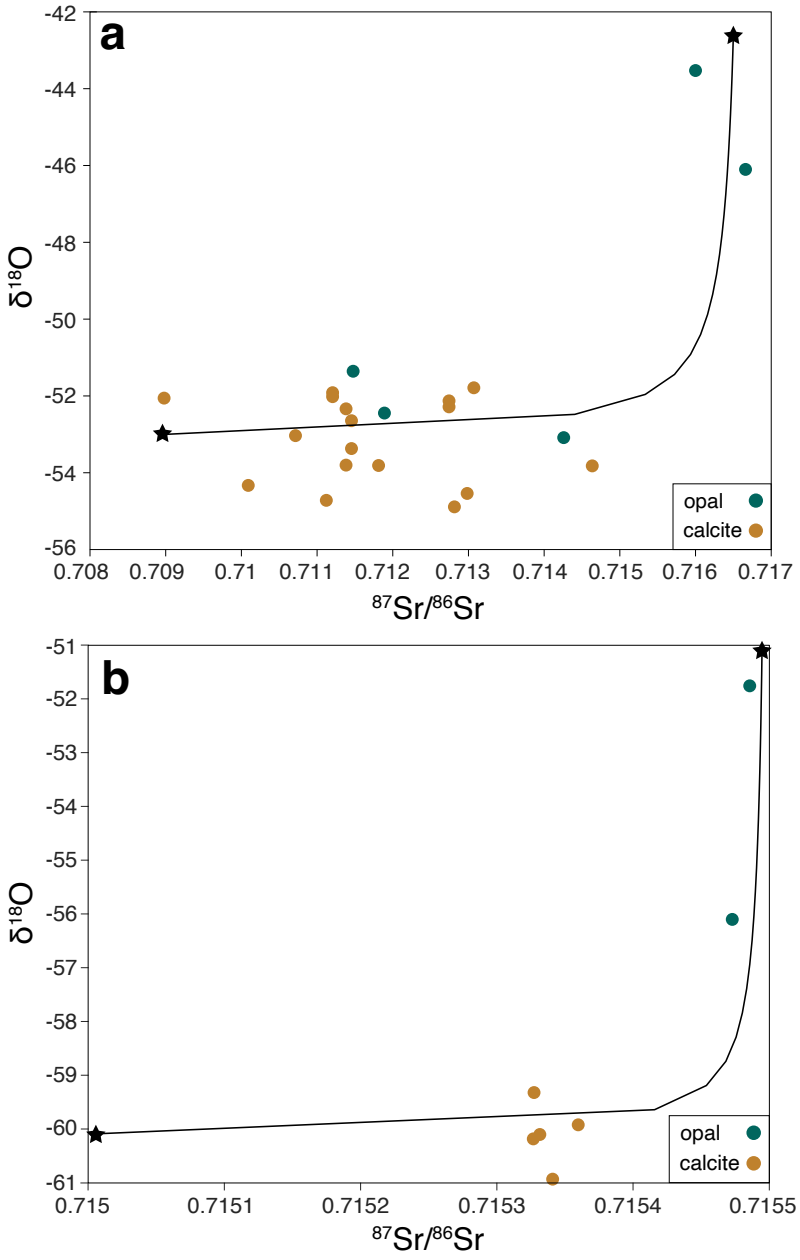

Extended Data Fig. 10 | Radiogenic Sr versus stable O isotope mixing curve for precipitates PRR50489 and MA113. a. $\delta^{18}O$ versus $^{87}Sr/^{86}Sr$ plot for PRR50489 calcite (brown) and opal (blue). Endmembers (stars) include an opal precipitating fluid Sr-rich, reduced groundwater; and a calcite precipitating fluid that is a Sr-poor, oxidizing glacial meltwater. Solid curved line represents mixing model between the two endmembers[10]. To fit calcite data, mixing models require a 98:2 ratio of Sr concentration between the brine:meltwater. **b.** As in **a**, but data are from sample MA113. To fit calcite data, mixing models require a 99:1 ratio of Sr concentration between the brine:meltwater.

References:

1. Martin, J. E., Patrick, D., Kihm, A. J., Foit, F. F. & Grandstaff, D. E. Lithostratigraphy, tephrochronology, and rare earth element geochemistry of fossils at the classical pleistocene Fossil Lake area, south central Oregon. *J. Geol.* **113**, 139–155 (2005).
2. De Carlo, E. H. & Green, W. J. Rare earth elements in the water column of Lake Vanda, McMurdo Dry Valleys, Antarctica. *Geochim. Cosmochim. Acta* **66**, 1323–1333 (2002).
3. Green, W. J. & Canfield, D. E. Geochemistry of the Onyx River (Wright Valley, Antarctica) and its role in the chemical evolution of Lake Vanda. *Geochim. Cosmochim. Acta* **48**, 2457–2467 (1984).
4. Harris, H. J. H. & Cartwright, K. Hydrology of the Don Juan Basin, Wright Valley, Antarctica. *Antarct. Res. Ser.* **33**, 162–184 (1981).
5. Tréguer, P. *et al.* The silica balance in the world ocean: A reestimate. *Science (80-.).* **268**, 375–379 (1995).
6. Dreybrodt, W., Buhmann, D., Michaelis, J. & Usdowski, E. Geochemically controlled calcite precipitation by CO2 outgassing: Field measurements of precipitation rates in comparison to theoretical predictions. *Chem. Geol.* **97**, 285–294 (1992).
7. Dandurand, J. L. *et al.* Kinetically controlled variations of major components and carbon and oxygen isotopes in a calcite-precipitating spring. *Chem. Geol.* **36**, 299–315 (1982).
8. Blasco, J., Tabone, I., Alvarez-Solas, J., Robinson, A. & Montoya, M. The Antarctic Ice Sheet response to glacial millennial-scale variability. *Clim. Past* **15**, 121–133 (2019).
9. Greene, C. A., Gwyther, D. E. & Blankenship, D. D. Antarctic Mapping Tools for MATLAB. *Comput. Geosci.* **104**, 151–157 (2017).
10. Phillips, D. L. & Koch, P. L. Incorporating concentration dependence in stable isotope mixing models. *Oecologia* **130**, 114–125 (2002).